Pergamon

Int. J. Heat Mass Transfer. Vol. 37, No. 14, pp. 2047–2057, 1994

0017-9310/94 $7.00 + 0.00

0017-9310(94)E0070-B

Convection induced by inclined thermal and solutal gradients, with horizontal mass flow, in a shallow horizontal layer of a porous medium

D. M. MANOLE and J. L. LAGE†

Mechanical Engineering Department, Southern Methodist University, Dallas, TX 75275-0335, U.S.A.

and

D. A. NIELD

Department of Engineering Science, University of Auckland, Auckland, New Zealand

(*Received* 17 *February* 1993 *and in final form* 1 *February* 1994)

Abstract—A theoretical examination is made of convection, induced by applied thermal and solutal coplanar gradients inclined to the vertical and with net horizontal mass flux, in a shallow horizontal layer of a saturated porous medium. The horizontal components of these gradients induce a Hadley circulation superimposed on the net horizontal flow. The combined flow becomes unstable when the vertical components are sufficiently large. The solid matrix of the saturated medium is assumed adiabatic (heat capacity ratio/porosity = 1). A linear stability analysis is carried out, and calculations are made using Galerkin approximation for the various modes of instability. The orientation of the preferred mode and the other critical quantities are determined for representative parameter values. Our results, when complemented with results found in the literature for different parameter values, indicate that the horizontal gradient effect switches from stabilizing to destabilizing as the magnitude of the gradient increases.

1. INTRODUCTION

ALTHOUGH a large number of papers have dealt with the natural convection, in a horizontal layer, induced by either horizontal or vertical temperature gradients, very few have dealt with the more general situation of inclined temperature gradients. The case of convection in a viscous fluid has been treated by Weber [1, 2], Sweet *et al.* [3], Bhattacharyya and Nadoor [4] and Nadoor and Bhattacharyya [5], and that of convection in a porous medium by Nield [6, 7] and Nield *et al.* [8]. The problem is complex, and each of the above publications have dealt with the simplified problem of flow in the central section of a shallow horizontal layer, one whose height-to-length and height-to-breadth ratios are small, so that the effect of lateral walls is to confine the fluid but it is otherwise negligible. We believe that this simplified problem is paradigmatic for more complicated problems involving imposed inclined temperature gradients.

With one exception, the work to date has been concerned with the case of a Hadley circulation, with zero net flow. Nield [6] treated the extension to non-zero net horizontal flow. Also, of the above papers, the only one dealing with the double-diffusive situation, where both thermal and solutal gradients are applied, is that by Nield *et al.* [8]. The present paper deals with the double-diffusive situation with nonzero net horizontal flow. Now the possible parameter space to be explored is even larger than before and in order to do this rapidly we have again been content to use a low order Galerkin approximation, the order of accuracy of which has been determined in a previous work (Nield [7]). For this report we have been narrowly selective in our choice of parameters used for computation. We have dealt only with the case of coplanar imposed thermal and solutal gradients. We have considered only the case of Dirichlet type boundary conditions on the perturbation temperature and concentration. Here we have considered flow in a saturated porous medium, and have postponed study of the analogous problem of flow in a clear fluid, for which the differential equation system is of higher order and there is an extra parameter (the Prandtl number) to vary.

Our work is of relevance to various geological and environmental situations in which thermohaline convection in a porous medium is applicable, such as those referred to by Sarkar and Phillips [9].

† Author to whom correspondence should be addressed.

NOMENCLATURE

a	volumetric specific heat ratio
A	matrix element, equation (28)
c, C	dimensional and nondimensional concentration
D	solutal diffusivity
E, F, G	constants
g	gravity acceleration
$\mathbf{h}$	unitary vertical vector, equation (8)
H	layer height
i	imaginary unit number
j	trial function number
k	thermal conductivity
K	permeability
Le	Lewis number
N	buoyancy ratio
p, P	dimensional and nondimensional pressure
q, Q	dimensional and nondimensional net flow magnitude
R	thermal Rayleigh number
r, s	horizontal wavenumber components
S	solutal Rayleigh number
SR	horizontal thermal and solutal Rayleigh number
t	time
T	temperature
u, v, w	Darcy velocity components
U, V, W	nondimensional Darcy velocity components
x, y, z	Cartesian coordinates
X, Y, Z	nondimensional Cartesian coordinates.

Greek symbols

α	thermal diffusivity
β	gradient vector horizontal component
γ	expansion coefficient
δ	Kronecker delta
Δ	difference
ε	relative error
η	horizontal wavenumber
θ	nondimensional temperature
λ	group parameter, equation (17)
μ	dynamic viscosity
ρ	density
σ	frequency, equation (22)
τ	nondimensional time
ϕ	porosity
χ	specific heat
Ψ	horizontal angle measured from x-axis.

Superscripts

$\sim$	function of z only
$'$	perturbation variable.

Subscripts

C	concentration
f	fluid
H	horizontal
j	index
m	porous medium
R	thermal
s	steady state
S	solutal
SR	thermal and solutal
T	temperature
0	reference value
x, y	horizontal
z	vertical.

2. BASIC EQUATIONS

The situation considered is that illustrated in Fig. 1. The Cartesian axes are chosen with the z-axis vertically upwards and the x-axis in the direction of the net flow, of magnitude q. The porous medium occupies a layer of height H. The vertical temperature difference across the boundaries is ΔT and the vertical concentration difference is Δc. The imposed horizontal thermal and concentration gradient vectors are (β_{Tx}, β_{Ty}) and (β_{Cx}, β_{Cy}), respectively.

We assume that the Oberbeck–Boussinesq approximation is valid, and that flow in the porous medium is governed by Darcy's law. Accordingly the governing equations are

$$\nabla \cdot \mathbf{v} = 0, \tag{1}$$

$$0 = -\nabla p - (\mu/K)\mathbf{v} + \rho_f \mathbf{g}, \tag{2}$$

$$(\rho\chi)_m(\partial T/\partial t) + (\rho\chi)_f \mathbf{v} \cdot \nabla T = k_m \nabla^2 T, \tag{3}$$

$$\phi(\partial c/\partial t) + \mathbf{v} \cdot \nabla c = D_m \nabla^2 c, \tag{4}$$

$$\rho_f = \rho_0[1 - \gamma_T(T - T_0) - \gamma_c(c - c_0)]. \tag{5}$$

Here $(u, v, w) = \mathbf{v}, p, T$ and c are the seepage (Darcy) velocity vector, pressure, temperature and concentration, respectively. The subscripts m and f refer to the porous medium and the fluid, respectively. Also μ, ρ and χ denote viscosity, density and specific heat, while K and ϕ are the permeability and porosity of the medium, k_m and D_m are the thermal conductivity and solutal diffusivity of the medium, and γ_T is the thermal expansion coefficient and γ_C the corresponding solutal parameter. Notice that, although γ_C is normally a negative quantity, we prefer to maintain a symmetrical notation in here.

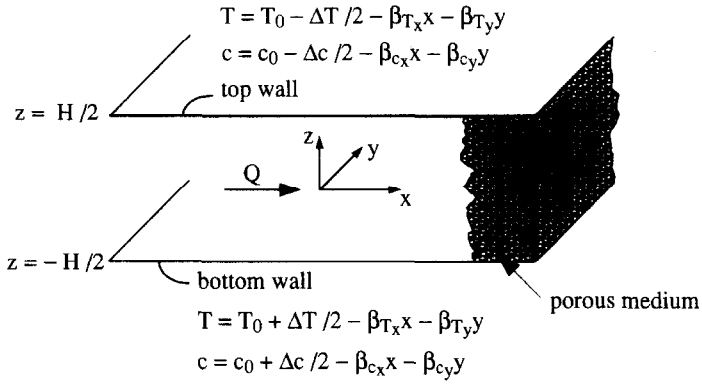

FIG. 1. Fluid saturated porous medium layer bounded by two horizontal impermeable solid surfaces.

The boundary conditions are

$$w = 0, \quad T = T_0 - (\pm\Delta T)/2 - \beta_{Tx}x - \beta_{Ty}y,$$
$$c = c_0 - (\pm\Delta c)/2 - \beta_{Cx}x - \beta_{Cy}y, \quad \text{at} \quad z = \pm H/2. \tag{6}$$

We define non-dimensional quantities by

$$(X, Y, Z) = \mathbf{X} = \mathbf{x}/H, \quad \tau = \alpha_m t/aH^2,$$
$$(U, V, W) = \mathbf{V} = H\mathbf{v}/\alpha_m, \quad P = K(p + \rho_0 gz)/\mu\alpha_m,$$
$$\theta = R_z(T - T_0)/\Delta T, \quad C = S_z(c - c_0)/\Delta c,$$

where

$$\alpha_m = k_m/(\rho_0\chi)_f, \quad a = (\rho\chi)_m/(\rho_0\chi)_f,$$
$$R_z = \rho_0 g\gamma_T KH\Delta T/\mu\alpha_m, \quad S_z = \rho_0 g\gamma_C KH\Delta c/\mu D_m.$$

We refer to R_z as the vertical thermal Rayleigh number and S_z as the vertical solutal Rayleigh number. In terms of the Lewis number $Le = \alpha_m/D_m$ and the buoyancy ratio $N = \gamma_C\Delta c/\gamma_T\Delta T$ we have $S_z = N\,Le\,R_z$. We also introduce horizontal thermal and solutal Rayleigh numbers defined by

$$R_x = \rho_0 g\gamma_T KH^2\beta_{Tx}/\mu\alpha_m,$$
$$R_y = \rho_0 g\gamma_T KH^2\beta_{Ty}/\mu\alpha_m,$$
$$S_x = \rho_0 g\gamma_C KH^2\beta_{Cx}/\mu D_m,$$
$$S_y = \rho_0 g\gamma_C KH^2\beta_{Cy}/\mu D_m.$$

The governing equations now take the form

$$\nabla\cdot\mathbf{V} = 0, \tag{7}$$
$$0 = -\nabla P - \mathbf{V} + (\theta + Le^{-1}C)\mathbf{h}, \tag{8}$$
$$\partial\theta/\partial\tau + \mathbf{V}\cdot\nabla\theta = \nabla^2\theta, \tag{9}$$
$$(\phi/a)\partial C/\partial\tau + \mathbf{V}\cdot\nabla C = Le^{-1}\nabla^2 C, \tag{10}$$

with $\mathbf{h}$ being the unit vector in the vertical direction. The boundary conditions are now

$$W = 0, \quad \theta = -(\pm R_z)/2 - R_x X - R_y Y,$$
$$C = -(\pm S_z)/2 - S_x X - S_y Y \quad \text{at} \quad Z = \pm 1/2. \tag{11}$$

The nondimensional net flow is defined as the Péclet number,

$$Q = qH/\alpha_m. \tag{12}$$

The scalings used for time and velocity, although somewhat arbitrary in the double-diffusive context, have the advantage of putting (9) in its simplest form and groups a and ϕ together in (10). It is noteworthy that (7)–(10) are dependent on R_z and S_z only through the boundary conditions, a consequence of the scalings that we use for temperature and concentration. The benefit of this approach is that all the Rayleigh numbers later appear in the perturbation equations via the steady-state solution only.

3. STEADY-STATE SOLUTION

Equations (7)–(11) have a steady-state solution of the form

$$\theta_s = \tilde{T}(Z) - R_x X - R_y Y, \quad C_s = \tilde{C}(Z) - S_x X - S_y Y,$$
$$U_s = \tilde{U}(Z), \quad V_s = \tilde{V}(Z),$$
$$W_s = 0, \quad P_s = P(X, Y, Z).$$

This is a solution provided

$$\frac{d\tilde{U}}{dZ} = R_x + S_x/Le,$$
$$\frac{d\tilde{V}}{dZ} = R_y + S_y/Le,$$
$$\frac{d^2\tilde{\theta}}{dZ^2} = -\tilde{U}R_x - \tilde{V}R_y,$$
$$Le^{-1}\frac{d^2\tilde{C}}{dZ^2} = -\tilde{U}S_x - \tilde{V}S_y.$$

The new flow specification, with Q aligned with the x-axis, requires that

$$\langle\tilde{U}\rangle = Q, \quad \langle\tilde{V}\rangle = 0.$$

Here the angle brackets denote an average with respect to the vertical coordinate, i.e. an integral with respect to Z from $-\frac{1}{2}$ to $\frac{1}{2}$.

The steady-state solution is thus

$$\tilde{U} = (R_x + S_x/Le)Z + Q, \tag{13}$$

$$\tilde{V} = (R_y + S_y/Le)Z, \tag{14}$$

$$\tilde{\theta} = -R_z Z + \tfrac{1}{24}\lambda_1(Z - 4Z^3) + \tfrac{1}{8}QR_x(1 - 4Z^2), \tag{15}$$

$$\tilde{C} = -S_z Z + \tfrac{1}{24}\lambda_2(Z - 4Z^3) + \tfrac{1}{8}Le\,QS_x(1 - 4Z^2), \tag{16}$$

where

$$\lambda_1 = R_x^2 + R_y^2 + (R_x S_x + R_y S_y)/Le,$$
$$\lambda_2 = S_x^2 + S_y^2 + Le(R_x S_x + R_y S_y). \tag{17}$$

The flow given by equations (13) and (14) with $Q = 0$ is commonly referred to as a Hadley circulation. We shall refer to the flow with $Q \neq 0$ as the "modified Hadley circulation".

We define the thermal and solutal Rayleigh number vectors by $\mathbf{R} = (R_x, R_y, R_z)$, $\mathbf{S} = (S_x, S_y, S_z)$. We note that here, with $Q \neq 0$, the modified Hadley circulation is no longer in the same vertical plane as that containing the vector $\mathbf{R} + \mathbf{S}/Le$.

4. STABILITY ANALYSIS

We now perturb the steady-state solution and write $\mathbf{V} = \mathbf{V}_s + \mathbf{V}', \theta = \theta_s + \theta', C = C_s + C', P = P_s + P'$. The linearized perturbation equations are

$$\nabla \cdot \mathbf{V}' = 0, \tag{18}$$

$$\nabla P' + \mathbf{V}' - (\theta' + C' Le^{-1})\mathbf{h} = 0, \tag{19}$$

$$\frac{\partial \theta'}{\partial \tau} + \tilde{U}\frac{\partial \theta'}{\partial X} + \tilde{V}\frac{\partial \theta'}{\partial Y} - R_x U' - R_y V' + \left(\frac{d\tilde{\theta}}{dZ}\right)W' = \nabla^2 \theta', \tag{20}$$

$$\left(\frac{\phi}{a}\right)\frac{\partial C'}{\partial \tau} + \tilde{U}\frac{\partial C'}{\partial X} + \tilde{V}\frac{\partial C'}{\partial Y} - S_x U' - S_y V' + \left(\frac{d\tilde{C}}{dZ}\right)W' = Le^{-1}\nabla^2 C'. \tag{21}$$

We make the normal mode expansion

$$[U', V', W', \theta', C', P'] = [U(Z), V(Z), W(Z), \theta(Z), C(Z), P(Z)] \times \exp\{i(rX + sY - \sigma\tau)\}. \tag{22}$$

We substitute this into the perturbation equations (18)–(21) and eliminate P, U and V from the resulting equations to obtain

$$\frac{d^2 W}{dZ^2} - \eta^2 W + \eta^2 \theta + \frac{\eta^2}{Le} C = 0, \tag{23}$$

$$\frac{d^2\theta}{dZ^2} + (-\eta^2 + i\sigma - ir\tilde{U} - is\tilde{V})\theta + i\eta^{-2}(rR_x + sR_y)\frac{dW}{dZ} - \left(\frac{d\tilde{\theta}}{dZ}\right)W = 0, \tag{24}$$

$$Le^{-1}\frac{d^2 C}{dZ^2} + (-Le^{-1}\eta^2 + i(\phi/a)\sigma - ir\tilde{U} - is\tilde{V})C + i\eta^{-2}(rS_x + sS_y)\frac{dW}{dZ} - \left(\frac{d\tilde{C}}{dZ}\right)W = 0, \tag{25}$$

where $\eta = (r^2 + s^2)^{1/2}$ is the overall horizontal wavenumber. We define the wavenumber vector by $\boldsymbol{\eta} = (r, s, 0)$.

The last three equations must be solved subject to appropriate boundary conditions. For the case of impermeable, isothermal, isosolutal boundaries we have

$$W = \theta = C = 0 \quad \text{at} \quad Z = \pm\tfrac{1}{2}. \tag{26}$$

The problem is now reduced to that of solving the equations (23)–(26), where

$$\frac{d\tilde{T}}{dZ} = -R_z + \frac{1}{24}\lambda_1(1 - 12Z^2) - QR_x Z,$$
$$\frac{d\tilde{C}}{dZ} = -S_z + \frac{1}{24}\lambda_2(1 - 12Z^2) - Q\,Le\,S_x Z. \tag{27}$$

For the particular case of $Le = \phi/a = 1$, the eigenvalue problem reduces to the same as for the monodiffusive case treated by Nield [6], but with R_x, R_y, R_z replaced by $R_x + S_x, R_y + S_y, R_z + S_z$, and with θ replaced by $\theta + C$.

In the general case, we may regard R_z as the eigenvalue, with Le, Q, ϕ, a, R_x, R_y, S_x, S_y, S_z, σ, r and s as parameters. The critical value of R_z is its minimum as σ, r, s are varied with s constrained so that R_z is real.

5. GALERKIN APPROXIMATION

Considering the large parameter space involved in the present study, it is convenient to employ a low order Galerkin approximation sufficiently accurate for the purpose in hand.

We select as trial functions, which satisfy the boundary conditions,

$$W_{2j-1} = \theta_{2j-1} = C_{2j-1} = \cos(2j-1)\pi Z, \tag{28}$$

$$W_{2j} = \theta_{2j} = C_{2j} = \sin 2j\pi Z, \tag{29}$$

$$\text{for } j = 1, 2, \ldots.$$

For the second order approximation, for example, we put

$$W = E_1 W_1 + E_2 W_2, \quad \theta = F_1\theta_1 + F_2\theta_2,$$
$$C = G_1 C_1 + G_2 C_2$$

and substitute into the three equations (23)–(25). We multiply the first equation by W_1, the second by θ_1, the third by C_1, repeat the process with W_2, θ_2, C_2, then integrate each term with respect to Z from $-1/2$ to $1/2$, perform some integrations by parts utilizing the boundary conditions, and eliminate the constants E_1, E_2, F_1, F_2, G_1 and G_2 from the resulting six homogeneous linear equations. We thus obtain the eigenvalue equation in the form

$$\det[A_{mn}] = 0, \tag{30}$$

where, for $m, n = 1, 2$,

$$A_{3m-2,3n-2} = \left\langle \frac{dW_m}{dZ}\frac{dW_n}{dZ} + \eta^2 W_m W_n \right\rangle,$$

$$A_{3m-2,3n-1} = -\eta^2 \langle W_m \theta_n \rangle,$$

$$A_{3m-2,3n} = -\eta^2 Le^{-1} \langle W_m C_n \rangle,$$

$$A_{3m-1,3n-2} = \left\langle \frac{d\theta}{dZ}\theta_m W_n - i\eta^{-2}(rR_x + sR_y)\theta_m \frac{dW_n}{dZ} \right\rangle,$$

$$A_{3m-1,3n-1} = \left\langle \frac{d\theta_m}{dZ}\frac{d\theta_n}{dZ} + (\eta^2 - i[\sigma - r\tilde{U} - s\tilde{V}])\theta_m \theta_n \right\rangle,$$

$$A_{3m-1,3n} = 0,$$

$$A_{3m,3n-2} = \left\langle \frac{d\tilde{C}}{dZ} C_m W_n - i\eta^{-2}(rS_x + sS_y) C_m \frac{dW_n}{dZ} \right\rangle,$$

$$A_{3m,3n-1} = 0,$$

$$A_{3m,3n} = \left\langle Le^{-1}\frac{dC_m}{dZ}\frac{dC_n}{dZ} + (Le^{-1}\eta^2 - i[\phi\sigma/a - r\tilde{U} - s\tilde{V}])C_m C_n \right\rangle.$$

The various integrals involved are easily evaluated. For example, one obtains

$$\langle W_m W_n \rangle = \delta_{mn}/2,$$

$$\left\langle \frac{dW_m}{dZ}\frac{dW_n}{dZ} \right\rangle = m^2\pi^2\delta_{mn}/2,$$

$$\langle Z\theta_m W_n \rangle = \frac{4mn\nu_{mn}}{\pi^2[m^2 - n^2]^2},$$

$$\langle Z^2\theta_m W_n \rangle = \left(\frac{1}{24} - \frac{1}{4\pi^2 n^2}\right)\delta_{mn},$$

$$\left\langle \theta_m \frac{dW_n}{dZ} \right\rangle = \frac{2mn\nu_{mn}}{n^2 - m^2},$$

where

$$\nu_{mn} = \begin{cases} 0 & \text{if } (m+n) \text{ is even,} \\ 1 & \text{if } (m+n+1)/2 \text{ is even,} \\ -1 & \text{if } (m+n+1)/2 \text{ is odd.} \end{cases}$$

Hence one finds that

$$A_{11} = (\pi^2 + \eta^2)/2, \quad A_{12} = -\eta^2/2,$$

$$A_{13} = -Le^{-1}\eta^2/2, \quad A_{14} = A_{15} = A_{16} = 0, \tag{31}$$

$$A_{21} = -R_z/2 + \lambda_1/8\pi^2, \quad A_{22} = (\pi^2 + \eta^2 - i(\sigma - rQ))/2,$$

$$A_{23} = 0, \quad A_{24} = -8R_x Q/9\pi^2 - 4i\boldsymbol{\eta}\cdot\mathbf{R}/3\eta^2,$$

$$A_{25} = 8i\{\boldsymbol{\eta}\cdot\mathbf{R} + Le^{-1}\boldsymbol{\eta}\cdot\mathbf{S}\}/9\pi^2, \quad A_{26} = 0, \tag{32}$$

$$A_{31} = -S_z/2 + \lambda_2/8\pi^2, \quad A_{32} = 0,$$

$$A_{33} = \{Le^{-1}(\pi^2 + \eta^2) - i(\phi\sigma/a - rQ)\}/2,$$

$$A_{34} = -8LeS_x Q/9\pi^2 - 4i\boldsymbol{\eta}\cdot\mathbf{S}/3\eta^2, \quad A_{35} = 0,$$

$$A_{36} = 8i\{\boldsymbol{\eta}\cdot\mathbf{R} + Le^{-1}\boldsymbol{\eta}\cdot\mathbf{S}\}/9\pi^2, \tag{33}$$

$$A_{41} = A_{42} = A_{43} = 0, \quad A_{44} = (4\pi^2 + \eta^2)/2,$$

$$A_{45} = -\eta^2/2, \quad A_{46} = -Le^{-1}\eta^2/2, \tag{34}$$

$$A_{51} = -8R_x Q/9\pi^2 + 4i\boldsymbol{\eta}\cdot\mathbf{R}/3\eta^2,$$

$$A_{52} = 8i\{\boldsymbol{\eta}\cdot\mathbf{R} + Le^{-1}\boldsymbol{\eta}\cdot\mathbf{S}\}/9\pi^2, \quad A_{53} = 0,$$

$$A_{54} = -R_z/2 + \lambda_1/32\pi^2,$$

$$A_{55} = (4\pi^2 + \eta^2 - i(\sigma - rQ))/2, \quad A_{56} = 0, \tag{35}$$

$$A_{61} = -8Le\,S_x Q/9\pi^2 + 4i\boldsymbol{\eta}\cdot\mathbf{S}/3\eta^2, \quad A_{62} = 0,$$

$$A_{63} = 8i\{\boldsymbol{\eta}\cdot\mathbf{R} + Le^{-1}\boldsymbol{\eta}\cdot\mathbf{S}\}/9\pi^2,$$

$$A_{64} = -S_z/2 + \lambda_2/32\pi^2, \quad A_{65} = 0,$$

$$A_{66} = \{Le^{-1}(4\pi^2 + \eta^2) - i(\phi\sigma/a - rQ)\}/2. \tag{36}$$

6. NUMERICAL PROCEDURE

We have developed a Fortran program to compute R_z so that we could search for the minimum (critical) value of R_z, as the horizontal wavenumber vector $\boldsymbol{\eta} = (r, s, 0) = \eta(\cos\Psi, \sin\Psi, 0)$ and the time frequency σ varies. We have capitalized on the fact that (30) is quadratic in R_z. This means that we can calculate approximations for the two lowest eigenvalues for any given set of parameter values. We are interested in the smallest real value of R_z, and hence in the smaller of the two real roots.

The process of finding the minimum R_z starts with writing the matrix A_{mn} in algebraic (symbolic) form. Then $\det[A_{mn}]$ is expanded using Mathematica, a symbolic manipulation software package, with all the coefficients written in rational form to enhance numerical accuracy. The resulting expression is factored with respect to powers of R_z in order to identify the coefficients of the quadratic equation in R_z. Each of these coefficients are then factored with respect to η and σ in that order. One finds that the real and imaginary parts of the coefficients of the powers of R_z have the general forms

$$\{\eta^{2n+1}Q\sigma(1 + \sigma^2 + Q^2) + \eta^{2n}(1 + \sigma^2 + \sigma^4 + Q^2 + Q^4)\}$$

and

$$\{\eta^{2n+1}Q(1 + \sigma^2 + Q^2) + \eta^{2n}\sigma(1 + \sigma^2 + Q^2) + \sigma(1 + \sigma^2)\},$$

respectively.

The algebraic expressions for the two roots are then put into a Fortran program and evaluated using double precision. Each R_z root is a function of eleven parameters,

$$R_z = f(\eta, \Psi, \sigma, R_x, S_x, R_y, S_y, S_z, Q, a/\phi, Le).$$

Considering the case of coplanar horizontal gradi-

ents, we present our results in terms of horizontal Rayleigh number vectors, using the transformation

$$R_x = R_H \cos \Psi_{SR}, \quad R_y = R_H \sin \Psi_{SR},$$
$$S_x = S_H \cos \Psi_{SR}, \quad S_y = S_H \sin \Psi_{SR}, \qquad (37)$$

where the horizontal angle Ψ_{SR} locates the vertical plane that contains both horizontal gradients. This angle is measured counterclockwise from the x-axis and obtained as

$$\Psi_{SR} = \operatorname{arc\,cot}\left(\frac{R_x}{R_y}\right) = \operatorname{arc\,cot}\left(\frac{S_x}{S_y}\right). \qquad (38)$$

Notice that equation (38) reveals the range of Ψ_{SR} from 0° to 180°. It follows from equation (37) that R_H and S_H are

$$R_H = \frac{R_x}{\cos \Psi_{SR}} \quad \text{and} \quad S_H = \frac{S_x}{\cos \Psi_{SR}}$$

if Ψ_{SR} is different than 90°, otherwise, $R_H = R_y$ and $S_H = S_y$.

For each evaluation of a R_z root, the values of S_z, R_H, Ψ_R and S_H and Ψ_S were selected. Within the σ range where $\mathrm{Im}(R_z) = 0$, the values of σ and the wavenumber parameters η, Ψ were varied to give the minimum value of $\mathrm{Re}(R_z)$. Here a non-real value of R_z indicates the nonexistence of any unstable mode for the particular parameter values. We utilized the fact that $\mathrm{Im}(R_z)$ is a fourth degree polynomial in σ. We found that, in most cases examined here, the smallest σ-root gave the smallest R_z.

We have restricted the values of R_H and S_H to those for which the second order Galerkin approximation can be expected to give results which are sufficiently accurate to be useful. We have found that a second-order approximation appears to give values of the critical vertical Rayleigh number accurate to within about 3% when both λ_1 and λ_2 are less than 1000, and QR_x/R_z and $Q\,Le\,S_x/S_z$ are not too large. The accuracy deteriorates rapidly for higher values of the magnitudes of λ_1 and λ_2. For instance, Table 1 presents the comparison between results obtained with a 2nd-order Galerkin approximation and results obtained with 3rd-, 4th- and 5th-order approximations, using the same trial functions, for the case $Q = \Psi_{SR} = S_z = 0$, $Le = R_H = 10$. The comparative parameter is the relative percentage error, ε, defined as

$$\varepsilon = \frac{|R_z^{2nd} - R_z^{ord}|}{R_z^{2nd}} \times 100\%, \qquad (39)$$

where R_z^{2nd} and R_z^{ord} are critical vertical thermal Rayleigh numbers obtained using, respectively, 2nd and higher order approximations. The main factor determining the accuracy appears to be the deviation from linearity of the basic thermal and solutal profiles.

The expressions for R_z are periodic in Ψ, with period 180°, only when $\Psi_{SR} = 0°$ or 180°. For these cases, we restrict the calculations to the interval $0° \leqslant \Psi \leqslant 180°$. All the other configurations have to be investigated considering the entire domain $0° \leqslant \Psi \leqslant 360°$. After locating the region containing the absolute minimum of R_z, we determined the minimum using a step-size which was typically 0.1° for Ψ and 10^{-6} for α, and, for the oscillatory modes, we determined σ to within 10^{-6}. Hence the numerical inaccuracy is much less than the inaccuracy arising from the Galerkin approximation.

Table 1. Comparison between critical values obtained with 2nd and higher order Galerkin approximation ($Q = \Psi_{SR} = S_z = 0$, $Le = R_H = 10$)

Order	S_H	R_z	σ	Ψ (degrees)	η	ε
2	1	44.602	0	90	3.1	0
3		44.587	0	90	3.1	0.0034
4		44.587	0	90	3.1	0.0034
5		44.587	0	90	3.1	0.0034
2	10	70.135	0	90	3.1	0
3		69.549	0	90	3.2	0.835
4		69.549	0	90	3.2	0.835
5		69.545	0	90	3.2	0.841
2	20	103.31	0	90	3.1	0
3		100.61	0	90	3.3	2.61
4		100.61	0	90	3.3	2.61
5		100.58	0	90	3.3	2.64
2	50	206.36	0	90	6.3	0
3		174.44	0	90	6.8	15.47
4		166.45	0	90	7.4	19.34
5		168.05	0	90	6.4	18.56

7. RESULTS

In the present study, we keep the Lewis number, Le, constant equal to 10 and $a/\phi = 1$ throughout the calculations. This Lewis number is roughly representative for experiments with a sugar–salt system. The transient parameter, a/ϕ, affects only the oscillatory modes. The value chosen for a/ϕ is also appropriate for that system. The angle Ψ_{SR} varies from 0° to 180° in 45° intervals, and the net flow, Q, covers the range 0–15. To study the vertical concentration gradient effect, we select the values 0, 10, 20, 50 and 100 for S_z.

We compare our computations, for $Q = 0$, against the results of Nield *et al.* [8], obtaining perfect agreement. As a double check, we perform calculations considering temperature gradients only. Figure 2 presents critical vertical Rayleigh numbers, side by side with the ones obtained by Nield [6] using polynomial trial functions, for varying Q. The results are in general good agreement. The result obtained by Nield [7] for the monodiffusive situation, that there are no unstable longitudinal (with respect to the applied horizontal gradient) oscillatory modes for the case of zero Q, holds also for nonzero Q. This can be demonstrated by putting $r = 0$ (and also $R_y = S_x = S_y = S_z = 0$, and Le tending to infinity) in equation (30), expanding the determinant, taking the real and imaginary parts of the equation, and eliminating R_z from the resulting two equations. One can thus express σ^2 as the negative

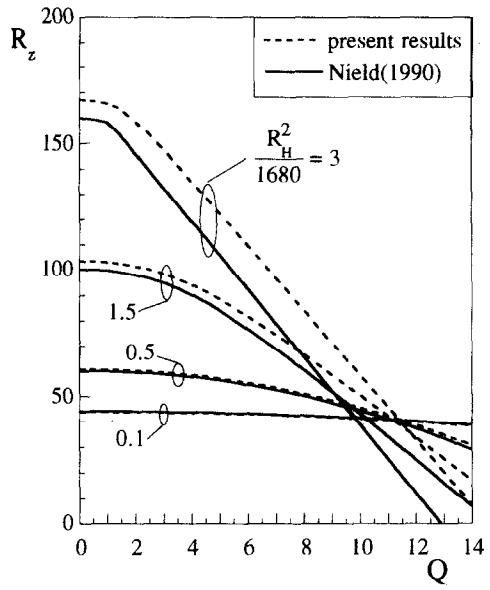

FIG. 2. Comparison of values of the critical Rayleigh number with results from Nield (1990).

of the sum of two squared expressions, and this implies that sigma can have no nonzero real value. (The earlier argument, in Nield [6], is inadequate.) We agree with Nield's [7] conclusion that the stabilizing effect of R_H deteriorates when Q increases beyond a certain limit value. However, our results indicate a weaker effect of R_H upon Q-limit with the former being almost constant and approximately equal to 11.4.

In Fig. 3, we compare the evolution with Q of the critical Rayleigh number, R_z, for three different Ψ_{SR} values, namely 0°, 45° and 90°, with R_H equal to 1 and S_H equal to 10. The arrows indicate the direction of S_z increase, from 0 to 100. It is noteworthy that by using ($Q \cos \Psi_{SR}$) instead of Q as abscissa the curves for $\Psi_{SR} = 45°$ fall on top of the curves for $\Psi_{SR} = 0°$. Moreover the net flow seems to have no effect, for the considered Q range, on the stability of the system when $\Psi_{SR} = 90°$. This indicates that, for small Q, it is the component of the net horizontal flow in the direction of the applied thermal and solutal gradients which has the major effect on the stability. The curves are smooth, with critical mode switching between oscillatory and nonoscillatory, the later predominating at small Q as Ψ_{SR} tends to 0°. The coplanar angle, Ψ_{SR}, has a stabilizing effect as it goes from 0° to 90° (or destabilizing from 90° to 180°) for constant Q. For all cases, larger concentration Rayleigh numbers, S_z, have an increasing destabilizing effect, as expected. Note that the curves are displaced vertically by approximately the amount in which S_z changes, so that the effects of R_z and S_z are approximately additive.

The horizontal thermal Rayleigh number effect, for $S_H = 10$ and $\Psi_{SR} = 0°$, is exemplified in Fig. 4. Here, we plot the critical Rayleigh numbers for three R_H values, for Q equal to 2 and 5. Important observations from this figure include: the linear relationship between R_z and S_z (observe that, except for the oscillatory mode when S_z is small, all curves have the same inclination), and the stabilizing effect of R_H when R_H goes from negative to positive values (from opposite to same orientation as Q).

Figure 5 focuses upon the S_H effect, with $R_H = 10$, Ψ_{SR} equal to 0° (top) and 90° (bottom), and S_z equal to 0 (left), 20 (center) and 100 (right). Notice that results for $S_H = \pm 100$ are included mainly to show the qualitative trends since, as pointed out previously, for these high values our 2nd-order approximation yields much lower accuracy. For the considered Q range, the net flow has a small effect on the stability of the system when $\Psi_{SR} = 90°$, with the destabilizing net flow effect being reduced as Ψ_{SR} tends to 90°. In the top row graphs, we identify the dual effect of increasing S_H. Consider for instance $S_z = 20$, a case shown by the top-center graph. As S_H increases from 0 to 10, the system becomes more stable if $Q < 4$ and more unstable if $Q > 4$. This behavior mimics the R_H effect found by Nield [6] when studying net flow with thermal horizontal gradient only. To better understand the S_H effect, we present Fig. 6, for $\Psi_{SR} = 0°$, $R_H = 10$, and S_z from 0 to 100. In here, we plot R_z against S_H, for various Q values. The dual effect is observed for the curves with horizontal tangent: $Q \leqslant 1$ for $S_z = 0$, $Q \leqslant 2$ for $S_z = 20$, and $Q \leqslant 3$ for $S_z = 100$. The dashed lines in the bottom graphs (which are details of the top graphs) link the locations of maximum R_z (S_H dual) for each Q. Numerical values of S_H dual as a function of Q allow us to build Fig. 7. With a fixed Q, for each S_z curve, values of S_H above or below the curve lead to smaller critical R_z.

An important issue revealed by the previous results is the net flow directional effect. In our analysis, we consider the net flow direction as fixed and aligned with the x-axis, and the coplanar horizontal gradient direction, Ψ_{SR}, as variable.

The net flow has two distinct effects. One of them is similar to the one indicated by Nield [7] for inclined horizontal thermal gradient with no net flow: the energy of the disturbance is modified by a transfer of energy due to the interaction of the perturbation convective motion with the basic gradient. The same reasoning can be extended in here. Equations (27) show that Q can distort both, thermal and solutal, basic gradients, affecting the transfer of energy. When Q increases, its effects on the basic temperature and concentration gradients will be to decrease them within the bulk of fluid and to increase them near the boundaries. Notice that increasing a gradient is destabilizing if the relative expansion coefficient is positive (R_z or $S_z > 0$) or stabilizing if the coefficient is negative (R_z or $S_z < 0$).

The second effect of the net flow Q is to distort the basic flow field, namely the Hadley flow, as seen in equation (13). This effect is always destabilizing since the composite flow ("modified Hadley circulation") has increased fluid motion near one of the horizontal

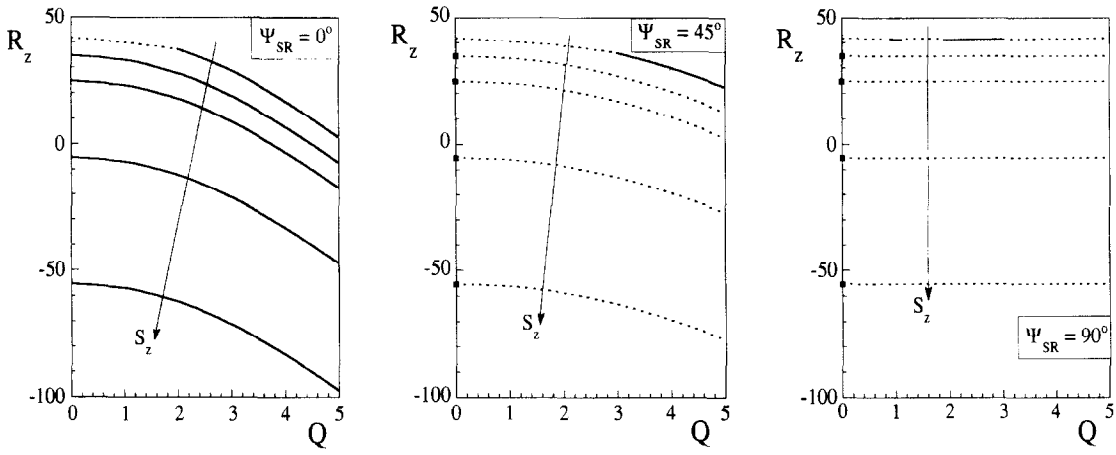

FIG. 3. Effect of coplanar angle on critical vertical Rayleigh number for $R_H = 1$ and $S_H = 10$. Nonoscillatory mode: continuous lines and black square; oscillatory mode: dashed lines. Arrows indicate increasing S_z: 0, 10, 20, 50, 100.

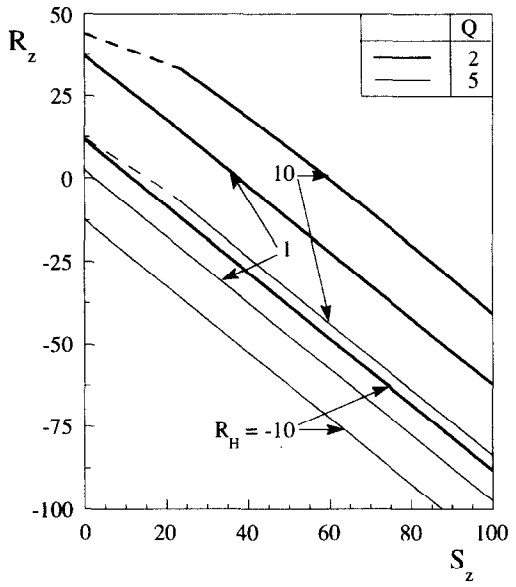

FIG. 4. Critical vertical Rayleigh numbers for $S_H = 10$.

boundaries (near the horizontal boundaries both gradients are largest, see equation (27)). The destabilization strength as Q increases is determined by the comparative strength of thermal and solutal gradients (recall that in this paper the large thermal and solutal gradients can be stabilizing or destabilizing depending on the expansion coefficient). That is why, in Fig. 5 top, increasing Q has a stronger destabilizing effect when S_H is large as shown by the inclination for $S_H = 10$ being steeper than for $S_H = -10$.

An explanatory comment is now made about an effect that is perhaps unexpected, namely the destabilizing effect (in some circumstances) of large Q even when perpendicular to the coplanar gradients ($\Psi_{SR} = 90°$). Examination of Fig. 5 shows that this effect is in fact a reduction in the stabilizing effect of the horizontal gradients, rather than a separate destabilization *per se*. When $\Psi_{SR} = 90°$ the effect of Q on the basic vertical temperature and concentration gradients, see equation (27), is zero, but, if r is not zero, Q still has an effect on the stability problem via its contribution to the modified Hadley flow; see equations (13), (24) and (25). The relevant situation is one for which R_H and S_H are both positive. In thermohaline terms, this means that the unmodified Hadley flow involves the movement of hotter, fresher (and hence less dense) water over cooler, saltier water, a situation that is stable. The effect of increasing Q is to increase the deviation of the alignment of the modified Hadley flow from that of the unmodified flow. The component of each applied horizontal gradient in the direction of the flow is reduced, and it appears that at some stage this is accompanied by a reduction in stability. At the same time the relation between the growth rates of different disturbance is altered. Our results show that for the unmodified flow an oscillatory mode is favoured, but a nonoscillatory mode is favoured when Q is large. We note that the favoured disturbance is one for which Ψ is zero (or 180°); this confirms that r is not zero. This means that the streamlines for the perturbation flow are in the (x, z) plane.

Using the definition of horizontal temperature and concentration gradient vector, **SR**, in equation (40), a longitudinal mode is now defined to be one for which η is perpendicular to **SR**, and a transverse mode when η and **SR** are parallel. Note that this definition is different than the one used previously by Nield [6, 7] and Nield *et al.* [8] based on the velocity vector $(U, V, 0)$ and η. However, both definitions yield the same results for the case $Q = 0$, in which the velocity vector and **SR** are parallel; see equations (13) and (14). This is also true for the case $r = V = 0$ and $Q \neq 0$.

As indicated by the results reported previously in Table 1, the favored modes are in general longitudinal. Recalling that Ψ and Ψ_{SR} are the angles between the

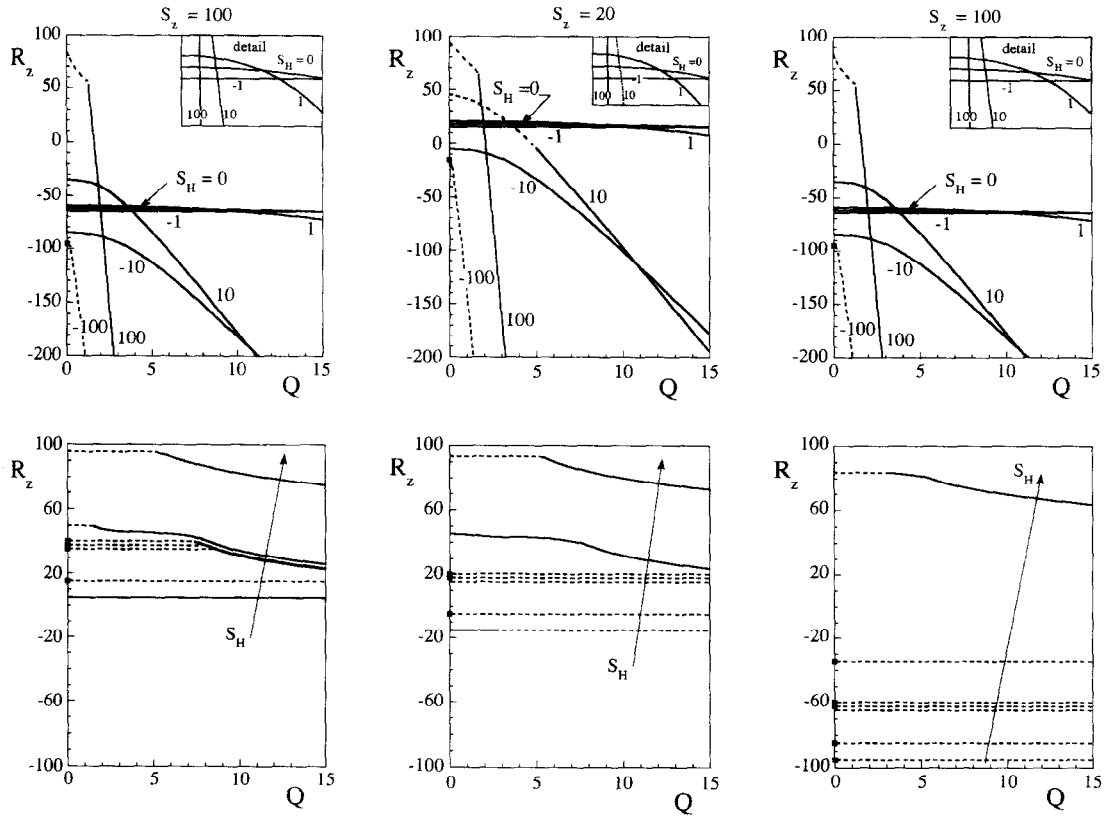

FIG. 5. Vertical concentration gradient effect on critical vertical Rayleigh number for $R_H = 10$, Ψ_{SR} equal to 0° (top) and 90°. Bottom graphs arrows indicate increasing S_H: -100, -10, -1, 0, 1, 10, 100.

x-axis and, respectively, the horizontal wavenumber vector and the co-planar gradient vector, the longitudinal and transverse modes directions are, respectively

$$\Psi = \Psi_{SR} \pm 90° \tag{40}$$

$$\Psi = \Psi_{SR}, \quad \text{or} \quad \Psi = \Psi_{SR} + 180°. \tag{41}$$

Equation (40), for longitudinal mode, helps explain once more why, even when the imposed horizontal gradients becomes perpendicular to the net flow, Q has an effect on critical R_z, as seen in Fig. 5. Recall that the perturbations can have any orientation; that means they can act also in the direction of the net flow Q. As mentioned before, we generally obtain longitudinal favored modes, i.e. the perturbations are precisely in the same direction as Q. Exceptions include, for instance, some oblique modes occurring for large S_H values as indicated in Table 2.

One of the reviewers has suggested a comparison between our results and results available in the literature, specifically the ones for a similar problem presented by Sarkar and Phillips [9]. Although it is always instructive to make comparisons with existing results, we justify in this section why this is not possible in the present case, unfortunately. We do, however, reconcile an apparent discrepancy pointed out by the same reviewer between our conclusions and the conclusions reached by Sarkar and Phillips [9]. It is easy to verify that their definition of horizontal gradient, R_x (p. 1167 of their paper), can be written as:

$$R_x = S_H + R_H = S_H\{1-(1/Le)\}, \tag{42}$$

where S_H and R_H are our horizontal thermal and solutal gradients, and Le is our Lewis number (notice that the Lewis number defined by Sarkar and Phillips [9] is equivalent to our Lewis number times porosity, ϕ Le). In their model, Sarkar and Phillips [9] imposed the mutually compensating horizontal gradients constraint (third line of their equation (1)), written, using our nomenclature, as:

$$\gamma_T \beta_{Tx} = -\gamma_C \beta_{Cx}, \tag{43}$$

so their analysis is less general than the ones presented in here. Furthermore, they assumed $(\phi\, Le) \sim 100$ and $\phi \sim 0.1$, and this implies that $Le \sim 1000$. It follows that their horizontal gradient can be written as: $R_x = 0.999 S_H$. In other words, they are effectively solving for relatively small horizontal temperature gradient ($R_H = -S_H/1000$) case as stated in their paper.

Sarkar and Phillips' [9] analysis is accurate for large horizontal gradient values, $R_x > 1000$, that in our case translates into $S_H > 1000$. However, as we have pointed out previously, the accuracy of our analysis deteriorates very rapidly as S_H increases. We conclude then that both analyses are clearly complementary: it is unreasonable to perform the comparison suggested

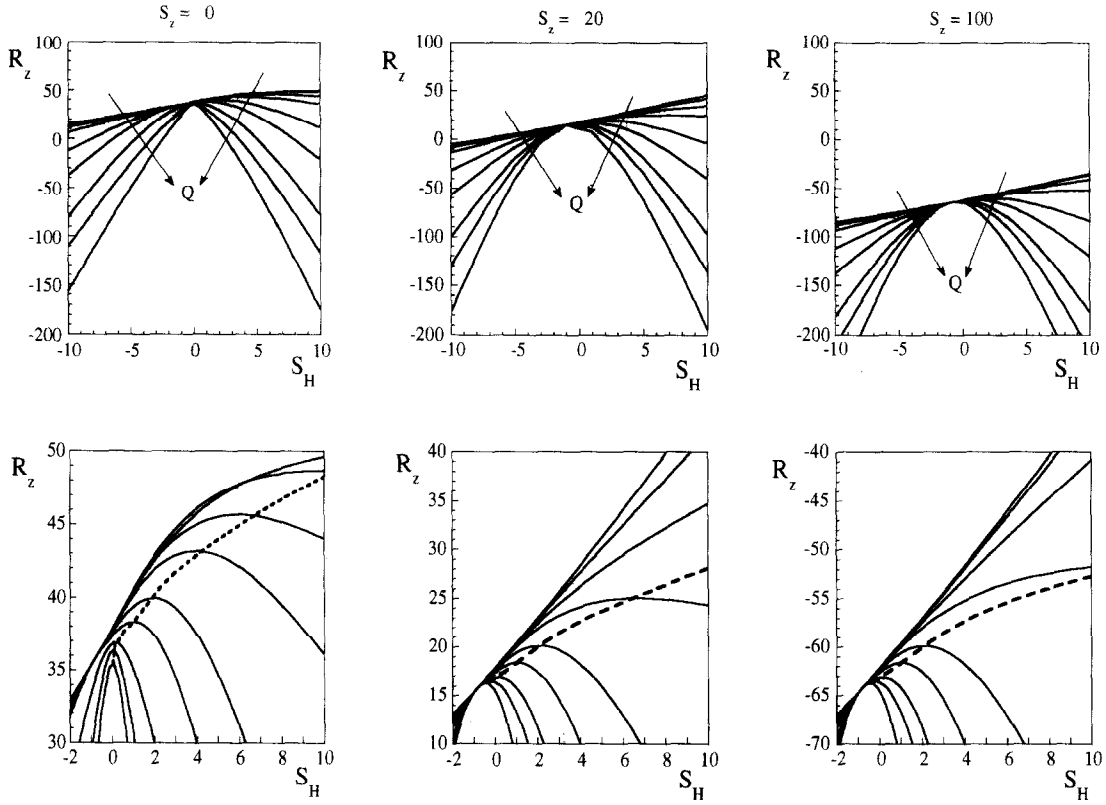

FIG. 6. Effect of net mass flow rate, Q, on critical vertical Rayleigh number for $\Psi_{SR} = 0°$, and $R_H = 10$. (Arrows indicate increasing Q: 0, 1, 2, 3, 5, 7, 10, 12, 15; bottom graph shows detail of top graph.)

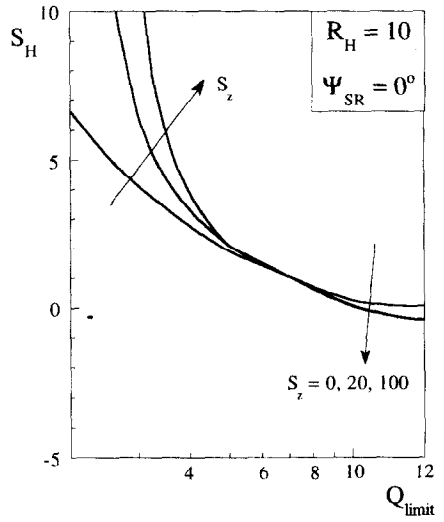

FIG. 7. Dual effect: locating the triplet (S_H, Q, S_z) for maximum critical horizontal Rayleigh number.

Table 2. Critical vertical Rayleigh number, frequency, and wavenumber magnitude and direction for selected configurations ($Q = 5, S_z = 0, Le = R_H = 10$)

Ψ_{SR}	S_H	R_z	σ	η	Ψ (degrees)
0°	−10	−11.9	0	4.21	90
	−1	41.8	0	3.99	90
	0	43.8	0	3.99	90
	1	44.7	0	3.99	90
	10	17.1	18.4	3.51	44
45°	−10	3.36	13.6	3.85	315
	−1	39.7	11.1	3.14	315
	0	43.8	11.3	3.19	315
	1	42.9	14.1	3.15	315
	10	30.8	15.2	3.61	63
90°	−10	19.2	16.9	3.37	0
	−1	39.5	15.7	3.14	0
	0	42.0	15.7	3.14	0
	1	43.4	15.7	3.13	0
	10	45.4	18.5	3.14	180
			0		

by the reviewer since the accuracy limitations are very distinct and non-overlapping. We can, however, draw a parallel between the conclusions from both analysis. We will show that the results are not in disagreement but, on the contrary, are complementary to each other.

The main conclusion of Sarkar and Phillips [9] (the one questioned by the reviewer) has to do with the horizontal concentration gradient being always destabilizing. Of course this is true within the calculation range used by them, that translates roughly into: $S_H > 1000$. Our results, as seen in Fig. 6 for $S_z = 0$, $Q = 0$, $Le = 10$, $R_H = 10$, and S_H from −10 to 10, shows that as S_H increases, R_z also increases (stabilizing effect), leading to an apparent contradiction.

It is important to stress the "apparent contradiction" here since it is obvious that the ranges used by either study are quite different (two orders of magnitude!) and that our results are not restricted by the mutually compensating horizontal gradients constraint. We made some additional computations for $R_H = -S_H/Le$, that satisfies the condition of mutually compensating horizontal gradients, as imposed by Sarkar and Phillips [9]. For $Q = S_z = 0$, $Le = 10$, and $1 \leqslant R_H \leqslant 10$. Our results show, for this particular case, that increasing R_H its effect is always destabilizing, extending Sarkar and Phillips' [9] conclusion for low R_H value range.

It is worth noting that our results in Fig. 6 also show that the rate of R_z increase is clearly reduced as S_H increases. Notice that for larger Q, the S_H effect goes from stabilizing to destabilizing. We can speculate then that, for larger S_H and for $Q = 0$, there will be a turning point beyond which the S_H effect is changed from stabilizing to nonstabilizing. Unfortunately our low order Galerkin approximation is not accurate enough to show the turning point for $Q = 0$. We point out, however, the recent analysis of horizontal inclined thermal gradient performed by Nield [10] employing an 8th-order Galerkin approximation. His results clearly indicate that the horizontal gradient has a dual effect on the base flow, the critical vertical Rayleigh increasing as R_H increases from 0 to 80 but then decreasing as R_H increases further.

8. CONCLUSION

Our theoretical examination of convection induced by applied coplanar thermal and solutal gradients inclined to the vertical revealed the destabilizing effect of a net horizontal mass flux superimposed to the original Hadley circulation. Furthermore, our results indicate that high enough net mass flux, Q, can have an effect on the critical Rayleigh number even when the horizontal gradients are perpendicular to the direction of the mass flux. The effect of increasing the positive vertical solutal Rayleigh number, S_z, is always destabilizing while increasing the horizontal thermal gradient, R_H, is stabilizing for the parameter range investigated. We also found a dual effect of the horizontal concentration gradient, S_H, on the vertical critical Rayleigh number: increasing S_H has a stabilizing effect on the system, maximum at $Q = 0$, that decreases as Q increases up to a critical value beyond which the system becomes increasingly unstable.

Acknowledgements—D. M. Manole acknowledges with gratitude the Ph.D. scholarship provided by the Mechanical Engineering Department of Southern Methodist University. Prof. Lage's work is supported by the J. L. Embrey Professorship in Mechanical Engineering. We are also indebted to the reviewers for their enlightening comments and suggestions.

REFERENCES

1. J. E. Weber, On thermal convection between non-uniformly heated planes, *Int. J. Heat Mass Transfer* **16**, 961–970 (1973).
2. J. E. Weber, On the stability of thermally driven shear flow heated from below, *J. Fluid Mech.* **87**, 65–84 (1978).
3. D. Sweet, E. Jakeman and D. T. J. Hurle, Free convection in the presence of both vertical and horizontal temperature gradients, *Physics Fluids* **20**, 1412–1415 (1977).
4. S. P. Bhattacharyya and S. Nadoor, Stability of thermal convection between non-uniformly heated plates, *Appl. Sci. Res.* **32**, 555–570 (1976).
5. S. Nadoor and S. P. Bhattacharyya, Hydromagnetic thermal convection between non-uniformly heated plates, *Acta Mech.* **41**, 265–282 (1981).
6. D. A. Nield, Convection in a porous medium with inclined temperature gradient and horizontal mass flow, *Heat Transfer* 1990, Hemisphere **5**, 153–185 (1990).
7. D. A. Nield, Convection in a porous medium with inclined temperature gradient, *Int. J. Heat Mass Transfer* **34**, 87–92 (1991)
8. D. A. Nield, D. M. Manole and J. L. Lage, Convection induced by inclined thermal and solutal gradients in a shallow horizontal layer of a porous medium. *J. Fluid Mech.* **257**, 559–574 (1993).
9. A. Sarkar and O. M. Phillips, Effects of horizontal gradients on thermohaline instabilities in a thick porous layer, *Physics Fluids A* **4**, 1165–1175 (1992).
10. D. A. Nield, Convection in a porous medium with inclined temperature gradient: additional results, *Int. J. Heat Mass Transfer* (in press).